On Wavenumber Estimates for Forced Continental Shelf Waves

RICHARD E. THOMSON

Institute of Ocean Sciences, Sidney, B.C. V8L 4B2, Canada

JASON H. MIDDLETON

Faculty of Science, University of New South Wales, Kensington, N.S.W., Australia

(Manuscript received 30 September 1983, in final form 2 October 1984)

ABSTRACT

We derive expressions that predict the variations of Cartesian, rotary and elliptical properties of free and forced barotropic continental shelf waves as functions of alongshore and cross-shore location. Bottom friction is shown to significantly complicate these expressions. Particular attention is given to the spatial variability in the phases of forced waves as functions of the wavenumbers of the forcing and the corresponding free wave mode. Consideration of the alongshore and across-shelf structure predicted by the theory indicates that, for a given frequency, the relative merits of Cartesian or rotary Fourier analysis of data depends on the location of the observation stations in the across shelf direction and on the geometry of the continental shelf and slope. The specific case of observed, diurnal period (K_1) continental shelf waves off Vancouver Island is used to illustrate how the free and forced shelf wave models lead to different interpretations for the wavelengths of the free wave component. The results demonstrate the nontrivial nature of the forced problem and emphasize the need for accurate resolution of the wavenumber of the driving mechanism.

1. Introduction

Continental shelf waves have been the subject of considerable research since their discovery by Hamon in 1962. Documentary evidence for such coastally-trapped subinertial oscillations is now available for many regions of the world oceans and theoretical studies into the nature of the waves has continued almost unabated over the past two decades (Allen, 1980; Mysak, 1980). It is generally accepted that shelf waves are generated primarily by the alongshore wind stress and by tidal currents associated with the surface tide. Despite this, however, most investigators have tended to concentrate on freely propagating waves. (Among the few exceptions are Adams and Buckwald, 1969; Gill and Schumann, 1974; Csanady, 1978; and Thomson and Crawford, 1982.) The forced shelf wave problem has not been thoroughly addressed and therefore remains of considerable importance in physical oceanography. Moreover, conclusive evidence for directly-forced shelf wave motions has yet to be published and verification of shelf waves in current and sea level records continues to be based primarily on free mode analysis.

In practice, it is difficult to distinguish between forced and free shelf wave oscillations. The main reason for this is that the major driving mechanisms, such as the wind, can be expressed in terms of the free-wave cross-shelf eigenfunctions (Gill and Schumann, 1974). This means, for example, that the across-shelf contribution to a set of current observations is determinable without regard to the origin of the motions (Hsieh, 1982a, 1982b; Crawford and Thomson, 1982, 1984). Such is not the case for the alongshore structure of the waves. Here, the distinction between free and forced oscillations is essential if a given set of observations is to be correctly interpreted. The distinction is especially important when only alongshore measurements are available and the properties of possible shelf wave motions determined through estimates of points (ω, k) in frequency–wavenumber space (e.g., Middleton *et al.*, 1982; Middleton, 1983).

The principal aim at this paper is to relate the spatial difference in the phase of a forced shelf wave of given frequency with the wavenumbers of the forcing and the corresponding free shelf-wave mode. It is this relationship that is used when estimating the "wavelength" of observed shelf waves and, in certain cases, to verify the existence of these oscillations in a set of current or sea level observations. A secondary aim is to discuss the relative merits of rotary versus Cartesian representation of current vectors when determining alongshore wavenumber. The paper is organized as follows. In Section 2 we present an abbreviated derivation of the forced vorticity equation together with expressions for the streamfunction and velocity components. Analytical methods for shelf wave detection are outlined in Section 3. Solutions to the general problem are presented in Section 4 for

specific models of the forcing function and the appropriate relationships between phase and wavenumber subsequently derived. In Section 5, the specific case of tidally-forced, first-mode shelf waves of diurnal frequency is considered in detail, with emphasis on the rotary properties of the waves. A discussion and summary follow in Section 6.

2. Formulation

We consider a homogeneous ocean of uniform rotation rate f, variable depth $H(x)$ and uniform shelf width L bordered by a straight coastline and occupying the region $x \leq 0$, $-\infty < y < \infty$, $-H \leq z \leq 0$ (Fig. 1). Motions are assumed to be linear and hydrostatic. Provided the length scale L of the shelf waves is considerably less than the external deformation radius [i.e., $f^2L^2/(gH) \ll 1$], the rigid lid approximation can be made and a mass transport streamfunction ψ defined by

$$UH = \psi_y, \quad VH = -\psi_x, \tag{2.1}$$

where (U, V) are depth-averaged values of the instantaneous velocity components. Cross-differentiation of the horizontal momentum equations and the requirement that the alongshore scales greatly exceed the cross-shelf scales (i.e., $\partial/\partial y \ll \partial/\partial x$) leads to a wind-forced vorticity equation in ψ (Allen, 1980).

Solutions are obtained assuming that the cross-shelf component of transport vanishes at the coast and that the alongshore component of velocity vanishes beyond the seaward edge of the continental shelf. Here, we further assume that the alongshore component of the bottom stress $\tau_B{}^y$ decelerates the flow. Therefore any component of the bottom stress that might be capable of generating shelf wave motions (e.g., Thomson and Crawford, 1982) can be incorporated in a modified version of the stress $\tau_w{}^y$ which then includes both surface and bottom stress forcing mechanisms.

Bottom frictional effects on wind-generated shelf waves were discussed briefly by Gill and Schumann (1974). The first rigorous treatment of the problem was by Brink and Allen (1978) who demonstrated that friction damps the free wave component and reduces the phase lag between the alongshore component of the velocity and the wind relative to the frictionless case. Bottom friction also results in a cross-shelf phase lag with nearshore flow leading offshore flow for a given mode. This is not necessarily true, however, for the total response (Simons, 1983; Brink and Allen, 1983). When stratification is incorporated (Brink, 1982), there is a reduction in the effect of bottom friction and an added phase shift with depth. As with previous models, we consider friction to be small in the sense that the fractional attenuation in wave amplitude per unit wavelength is much less than unity.

A simple linear form for the bottom stress is

$$\tau_B{}^y = \rho_0 \nu v_z \approx \rho_0(\nu/\delta)V = \rho_0 r H^{-1}\psi_x, \tag{2.2}$$

where ν is a vertical eddy coefficient, $\delta = (2\nu/f)^{1/2}$ is the thickness of the bottom boundary layer and $r = \nu/\delta$ is a friction coefficient. Solutions to the vorticity equation for a stress of the form (2.2) have been presented by Brink and Allen (1978) for the case $r/fH_0 \to 0$, where H_0 is some scale depth (see also Brink and Allen, 1983).

Solutions for the above model are obtained using separation of variables and the assumption that the forcing term is independent of the cross-shore direction (Gill and Schumann, 1974). Substitution of

$$\psi(x, y, t) = \sum_{n=1}^{\infty} \Psi_n(y, t)\phi_n(x)$$

into the forced vorticity equation yields a Sturm-Liouville eigenvalue problem for the cross-shelf wave structure and a damped wave equation for the alongshore structure of mode n,

$$c_n{}^{-1}\Psi_{n,t} + \Psi_{n,y} + R_n\Psi_n = (b_n/\rho_0 f)\tau_w{}^y, \tag{2.3}$$

where the coefficient b_n is obtained from the orthogonality condition for ϕ_n (cf., Thomson and Crawford, 1982) and c_n is the phase speed. In the case of the bottom stress model (2.2), the friction coefficient

$$R_n = (fH_0)^{-1} r a_{nn}, \tag{2.4}$$

where

$$a_{nm} = H_0 \int_{-L}^{0} H^2 \phi_{m,x}\phi_{n,x} dx$$

(Brink and Allen, 1978). Our requirement for weak damping is that $R_n/k_n \ll 1$, where k_n is the alongshore wavenumber of the nth mode.

As stated previously, the function ϕ_n defining the cross-shelf structure of the waves is the same for both free and forced oscillations. A similar result is obtained for the stratified case (Brink, 1982) where $\phi_n(x) \to \phi_n(x, z)$ now incorporates both vertical and horizontal spatial structure. In coastal regions where horizontal variations in density could cause significant phase shifts over a wavelength, it may be necessary to

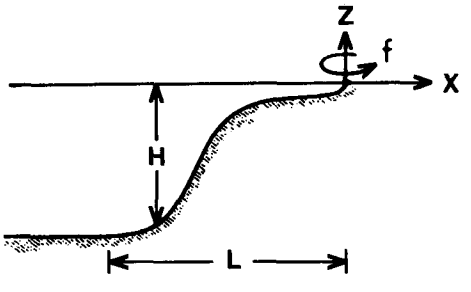

FIG. 1. Coordinate system. The alongshore direction (y) is into the page.

include stratification when comparing phase differences in currents.

Analytical solutions for ϕ_n are available for certain functional bottom topographies (e.g., Mysak, 1980) and numerical solutions can be obtained for functional or piecewise continuous depth profiles (e.g., Henry *et al.*, 1985). However, our interest is with the alongshore rather than the cross-shore wave structure so that ϕ_n is assumed known. Equation (2.3) is then solved using the method of characteristics for two basic types of forcing mechanisms: 1) the force vanishes prior to some starting location $y = y_0$ and 2) the force vanishes prior to some starting time $t = t_0$. Setting $\psi_n = 0$ at these positions, (2.3) yields

$$\Psi_n(y, t) = (b_n/f\rho_0)F_n(y) \times \int_{\eta_i}^{y} F_n^{-1}(\eta)\tau_w{}^y[\eta, c_n^{-1}(\eta - y) + t]d\eta, \quad (2.5)$$

where

$$F_n(y) = \exp\left(-\int^y R_n d\eta\right) \quad (2.6)$$

and where for cases (a) and (b) respectively, we have

$$\eta_i = y_0, \quad \eta_i = y_0 - c_n t_0. \quad (2.7)$$

In terms of the streamfunction (2.1), the horizontal velocity components are

$$(U_n, V_n) = H^{-1}(\phi_n \Psi_{n,y}, -\phi_{n,x}\Psi_n), \quad (2.8)$$

while the assumption that the alongshore flow is in the quasi-geostrophic balance, $g\eta_x \sim fV$, yields the sea level variations,

$$\zeta_n \approx \zeta(-L) - (f/g)\Psi_n \int_{-L}^{x} H^{-1}\phi_{n,x}dx. \quad (2.9)$$

3. Shelf wave detection

Numerous techniques exist for the detection of propagating shelf waves in simultaneously measured current or sea level records. For example, suppose we had a set of simultaneous current records from m cross-shelf locations. This allows up to $m - 1$ separate modes or wave types to be least squared fitted to the observations and provides estimates of the relative contribution of each mode to the total signal variance. The fitting could be based on the Cartesian velocity components (2.8) or on the rotary vector components (e.g., Hsieh, 1982a) and is possible irrespective of whether the waves are free or forced. To distinguish between the latter, it is best to have measurements in the alongshore direction. Moreover, in the case of wind-generated oscillations, it is imperative to have good enough spatial coverage of the wind to resolve the wavenumber of the prominent forcing.

Cross-spectral and cross-correlation analysis of observations spaced alongshore are often used to verify the presence of shelf wave motions and to provide estimates of wavenumbers (e.g., Middleton *et al.*, 1982). Cross-spectra or their normalized counterpart, coherence, yield the relative amplitudes and phases of two time-series records as a function of frequency while cross-correlation gives the alongshore time lag integrated over all frequenccy bands. If shelf wave oscillations are present in the observations, we expect to find significant peaks in the above functions with phase or time lags that are consistent with those obtained for calculated shelf waves (2.8) and (2.9).

We are concerned here with both Cartesian and rotary descriptions of motions in the complex plane (real equals across shelf; imaginary equals alongshore). The velocity vector $W = U + iV$ at a particular radian frequency ω may be written in the following forms

$$W = a\cos(\omega t + \alpha) + ib\cos(\omega t + \beta) \quad (3.1)$$

$$= A^+ e^{i(\omega t + \epsilon^+)} + A^- e^{-i(\omega t - \epsilon^-)} \quad (3.2)$$

$$= e^{i[(\epsilon^+ + \epsilon^-)/2]}\left\{(A^+ + A^-)\cos\left[\omega t + \left(\frac{\epsilon^+ - \epsilon^-}{2}\right)\right] + (A^+ - A^-)\sin\left[\omega t + \left(\frac{\epsilon^+ - \epsilon^-}{2}\right)\right]\right\}^2. \quad (3.3)$$

The Cartesian description (3.1) comprises two rectilinear components. The rotary description (3.2) comprises two contra-rotating circular components in the complex plane in which A^+ and A^- are the lengths of the rotary vectors while ϵ^+ and ϵ^- are the respective angles these vectors make with the x axis at time $t = 0$. The elliptical description (3.3) shows that the resultant of either (3.2) and (3.3) is an ellipse with major and minor axes of length $|A^+ + A^-|$ and $|A^+ - A^-|$, respectively. The major axis is oriented at angle $\theta = \frac{1}{2}(\epsilon^+ + \epsilon^-)$ from the x axis and the current vector rotates anticlockwise (clockwise) when $A^+ - A^-$ is positive (negative). The velocity vector is aligned with the major axis in direction θ when $\omega t = \frac{1}{2}(\epsilon^- - \epsilon^+)$.

Fourier coefficients found by use of the discrete Fourier transform may be used to obtain the Cartesian amplitudes and phases, the rotary amplitudes and phases or the relevant ellipse quantities. These calculations are usually made by means of the Fourier coefficients directly, or by the more common method of determining spectra, cross-spectra, coherence amplitude and coherence phase (Mooers, 1973; Calman, 1978; Middleton, 1982). For stationary, ergodic processes (which ocean currents are commonly assumed to be) there is an advantage of using spectral and coherence calculations (which require band or ensemble averaging in frequency space) in preference to individual Fourier coefficient calculations. This advantage is due to the fact that the distribution theory for these averaged quantities is known (Koopmans, 1974) allowing confidence limits to be placed on phase and amplitude estimates.

To compare phases between Cartesian components from two different locations, we usually use Cartesian coherence $C_{12}(\omega)$ and phase $\gamma_{12}(\omega)$. For example, for alongshore Cartesian velocity components of the form (3.1), the Fourier coefficients $\hat{V}(\omega)$ used to determine these quantities are of the form $\hat{V}(\omega) = \frac{1}{2}b \exp(i\beta)$ so that the phase is given by $\gamma_{12} = \beta_1 - \beta_2$. The orientation of ellipses and the phase differences between vector motions observed at different locations are found for the data using the rotary Fourier techniques which are applicable to (complex) vector series (e.g., Mooers, 1973). Coherences and phases in this case are determined for both positive and negative frequencies corresponding to anticlockwise and clockwise rotating components of the vector series. For a given frequency, there are four coherence amplitudes and associated phases linking "inner" and "outer" vector products. The phases ϵ^+ and ϵ^- in (3.2) and (3.3) for two vector series are related to the inner rotary coherence phase by

$$\gamma_{12}^{\pm}(\omega) = -\gamma_{21}^{\pm}(\omega) = \begin{cases} \epsilon_1^+ - \epsilon_2^+, & \omega > 0 \\ \epsilon_1^- - \epsilon_2^-, & \omega < 0, \end{cases} \tag{3.4}$$

while the difference in orientation between the major axes at frequency ω is

$$\theta_1 - \theta_2 = \frac{1}{2}[(\epsilon_1^+ + \epsilon_1^-) - (\epsilon_2^+ + \epsilon_2^-)]$$

$$= \frac{1}{2}[\gamma_{12}(+\omega) + \gamma_{12}(-\omega)]. \tag{3.5}$$

The difference in phases representing the time difference between the velocity vector of series 1 coinciding with its major axis and the velocity vector of series 2 coinciding with its major axis is given by the phase lag

$$\frac{1}{2}[(\epsilon_2^- - \epsilon_2^+) - (\epsilon_1^- - \epsilon_1^+)] = \frac{1}{2}[\gamma_{12}(+\omega) - \gamma_{12}(-\omega)]. \tag{3.6}$$

For a given mode and frequency, current ellipses of continental shelf waves possess marked across-shelf variation in amplitude, orientation and ellipticity. Consequently it is often more advantageous to analyse the currents in terms of their rotary components rather than Cartesian components (Hsieh, 1982). Close fits of observed to calculated ellipses provides convincing evidence for these waves. Similarly, separate estimates of the alongshore phase lag can be obtained from the clockwise and counterclockwise rotary components. Use of rotary components also avoids the difficulty of defining the alongshore direction, which arises when alongshore components are compared, and enables us to take advantage of the fact that first mode shelf waves are predominantly clockwise (anticlockwise) rotary over Northern (Southern) Hemisphere shelves, especially near the shelf break.

4. Shelf wave models

We now use the previous derivations to obtain shelf wave properties. Particular emphasis is on the spatial differences in the phases and ellipse orientations of free and forced waves. A number of forced models are considered. (As in Section 2, the analysis is for right-bounded waves in the Northern Hemisphere but can readily be adapted to left-bounded waves in the Southern Hemisphere.)

a. Free shelf waves

We begin with the case of free propagating waves along a uniform coastline in the presence of bottom friction. With $\tau_w^y = 0$, (2.3) yields

$$\Psi_n(y, t) = A(y - c_n t)F_n(y)$$

$$= A_0 \sin(ky - \omega t)F_n(y); \tag{4.1}$$

A_0 is the amplitude, $F_n(y)$ is defined by (2.7) and $\omega = kc$ is the wave frequency. Equation (4.1) combined with (2.8) then yields the Cartesian velocity components (dropping the subscript n),

$$U = a\phi(R^2 + k^2)^{1/2} \cos(ky - \omega t + \mu_0), \tag{4.2a}$$

$$V = -a\phi' \sin(ky - \omega t), \tag{4.2b}$$

where $' \equiv d/dx$, $a = A_0F/H$, $\mu_0 = \tan^{-1}(R/k)$ and, with $R \ll k$, $|k\phi/\phi'| \sim |U/V|$.

The amplitude and phases of the rotary velocity components are obtained by equating (3.2) and $W = U + iV$, using (4.2a,b); this yields

$$A^{\pm} = \frac{1}{2}a[(k\phi \pm \phi')^2 + R^2\phi^2]^{1/2}, \tag{4.3}$$

$$\epsilon^{\pm} = \mp\{ky + \tan^{-1}[R\phi/(k\phi \pm \phi')]\} + \pi m^{\pm}, \tag{4.4}$$

where plus corresponds to the anticlockwise and minus to the clockwise rotary component and where m^+ and m^- are positive integers. In any practical situation, the ambiguity in phase associated with the last term in (4.4) is removed by careful consideration of the observations. For undamped free waves ($R \equiv 0$), (4.4) simplifies to

$$\epsilon^{\pm} = \mp ky + \pi m^{\pm}. \tag{4.5}$$

Finally, the orientation θ of the major axis of the current ellipse to the x axis is, from (4.4) with $m^+ + m^- = m$,

$$\theta = \frac{1}{2}(\epsilon^+ + \epsilon^-)$$

$$= \frac{1}{2}m\pi + \frac{1}{2}\tan^{-1}\left[\frac{R(\phi^2)'}{(k^2 + R^2)\phi^2 - (\phi')^2}\right], \tag{4.6}$$

where we have made use of the trigonometric identity

$$\tan^{-1}\alpha - \tan^{-1}\beta = \tan^{-1}\left(\frac{\alpha - \beta}{1 + \alpha\beta}\right). \tag{4.7}$$

In the case of undamped waves, $\theta = \frac{1}{2}\pi m$ and the major axis is either normal ($\theta = 0°$) or parallel ($\theta = 90°$) to the shoreline. However, in general, bottom friction alters the currents to produce a cross-shelf modification of the ellipse orientation as given by the last term in (4.6). Over the inner continental shelf, currents are mainly alongshore (i.e., $|k\phi/\phi'| \ll 1$) and $\theta \approx 90°$. Large deviations in θ occur where the currents are nearly circularly polarized and ellipses are flipping orientation relative to the shore (cf., Fig. 3b).

Suppose we have simultaneous current velocity measurements from two alongshore locations y_1, y_2 and that phase propagation is from y_1 to y_2. In the present coordinate system, $y_2 > y_1$. Using (4.4) and (4.7), the principal parts of the phase differences (3.4) for the anticlockwise and clockwise rotary vectors are, then,

$$\gamma_{21}^{\pm} = \mp k(y_2 - y_1) + \tan^{-1}\left[\frac{R(\phi_1\phi_2' - \phi_2\phi_1')}{(k\phi_1 \pm \phi_1')(k\phi_2 \pm \phi_2') + R^2\phi_1\phi_2}\right]. \quad (4.8)$$

The alongshore phase differences are not only dependent on the wavenumber and alongshore separation distance but also on the magnitude of the frictional damping and the locations offshore where the measurements are obtained. In the inviscid case, (4.8) reduces to

$$\gamma_{21}^{\pm} = \mp k(y_2 - y_1), \quad k > 0. \quad (4.9)$$

The same expression (4.9) holds for $R \neq 0$ if ϕ or ϕ' vanish locally at both sites or if measurements are taken at the same distance offshore at both locations so that $\phi_1\phi_2' = \phi_2\phi_1'$. ($\phi' = 0$ implies $V = 0$.) Under these conditions the wavenumber and wavelength are given simply by

$$k = \gamma_{21}^{+}/(y_1 - y_2) = \gamma_{21}^{-}/(y_2 - y_1), \quad (4.10)$$

$$\lambda = 2\pi(y_2 - y_1)/|\gamma_{21}^{\pm}|. \quad (4.11)$$

In general, however, (4.8) must be considered in its entirety and k determined through a transcendental equation of the form $\tan[g(k; y)] = G(k; x)$.

The wavenumber can also be determined via the Cartesian velocity components (4.2) or the sea level fluctuations (2.9). In fact, there are quite distinct advantages in using these scalar quantities, as compared to the rotary or ellipse components, provided that the alongshore and cross-shore directions can be reliably determined. (The latter necessitates a comparatively straight coastline with parallel bottom contours.) Clearly, the phase differences for the individual velocity components are determined by the arguments of the cosine and sine functions in (4.2). The phase difference between alongshore components is then

$$\gamma_{21}^{\pm}(\omega) = \mp\tan^{-1}\left[\frac{\sin k(y_2 - y_1)}{\cos k(y_2 - y_1)}\right] = \mp k(y_2 - y_1) \quad (4.12)$$

and is identical to (4.9) for the undamped waves.

Comparison of the Cartesian and rotary component approaches suggests that, in general, it is more straightforward to use the velocity components separately when determining the relationship between alongshore phase difference and the wavenumber of free shelf waves. However, solutions to (4.8) are quite tractable and the rotary analysis method is useful for determination of the alongshore properties of free shelf waves. Morever, it is feasible in theory to use (4.12) to obtain an estimate of k which can then be substituted into (4.8) to obtain an estimate of the friction coefficient R. In practise, changes in alongshore topography, coastline orientation or stratification might mask any measured phase differences due to friction alone.

b. Traveling-wave forcing: Impulsive start time

The forcing function in this case has the form

$$\tau = \begin{cases} \tau_0 \cos(ky - \hat{\omega}t), & t > 0 \\ 0, & t < 0 \end{cases} \quad (4.13)$$

corresponding to a progressive forcing mechanism extending the entire length of a coast but starting impulsively at time $t = 0$. Substitution of (4.13) into (2.5) gives

$$\psi(x,y,t) = D_0\phi\left\{\frac{\omega - \hat{\omega}}{c}\left[\sin(ky - \hat{\omega}t) - \frac{F(y)}{F(y - ct)}\sin(ky - \omega t)\right] - R\left[\frac{F(y - ct)}{F(y)}\cos(ky - \omega t) - \cos(ky - \hat{\omega}t)\right]\right\},$$

in which

$$D_0 = \frac{\tau_0 b}{\rho_0 f}\left[\frac{c^2}{(\hat{\omega} - \omega)^2 + (Rc)^2}\right]^{1/2}$$

and $\omega = kc$ is the frequency of the free shelf wave. As usual, friction removes the singularity at resonance frequency $\hat{\omega} = \omega$.

The Cartesian and rotary velocity components are found as before. In the case of the former, we find:

$$U = dk\phi[\cos(\hat{\omega}t - ky + \hat{\mu}) - \cos(\omega t - ky + \mu)], \quad (4.14a)$$

$$V = d\phi'[\sin(\hat{\omega}t - ky + \hat{\mu}) - \sin(\omega t - ky + \mu)], \quad (4.14b)$$

in which

$$d = D_0/H; \quad \mu = \tan^{-1}\left[\frac{RcF^2(y - ct)/F^2(y)}{\hat{\omega} - \omega}\right];$$

$$\hat{\mu} = \tan^{-1}\left[\frac{Rc}{\hat{\omega} - \omega}\right].$$

Both components consist of damped forced and free waves of frequencies $\hat{\omega}$ and ω respectively. Therefore, for an impulsively started forcing field, current and sea level measurements made at a fixed location will reveal oscillations at two distinct frequencies. Moreover, the Cartesian and rotary representations of each of these oscillations can be expressed in a form similar to that of the free waves discussed in the previous section. Also, the wavenumber k is the same for both the free and forced wave so that the wavelength $\lambda = (2\pi/\gamma_{21})(y_2 - y_1)$ where, as before, γ_{21} is the phase difference between the two locations based on the Cartesian or rotary components. The results clearly suggest that impulsively generated local waves are well served by rotary decomposition in which the ellipse properties for each frequency are separately determined.

There are a number of additional features of the problem worth noting. Suppose $R = 0$ (i.e., $\mu = \hat{\mu} = 0$) and that we combine the free and forced wave components in (4.14a,b) in the form,

$$\left.\begin{aligned} U &= 2\bar{d}k\phi \sin\left[\tfrac{1}{2}(\omega - \hat{\omega})t\right] \sin\left[ky - \tfrac{1}{2}(\omega + \hat{\omega})t\right] \\ V &= 2\bar{d}\phi' \sin\left[\tfrac{1}{2}(\omega - \hat{\omega})t\right] \cos\left[ky - \tfrac{1}{2}(\omega + \hat{\omega})t\right] \end{aligned}\right\},$$

where

$$\bar{d} = \frac{\tau_0 b}{\rho_0 f H}\frac{c}{(\hat{\omega} - \omega)}.$$

The velocity components in this representation consist of temporally modulated travelling waves with effective frequency $\omega_e \equiv \frac{1}{2}(\omega + \hat{\omega})$ and effective phase speed $c_e \equiv \frac{1}{2}(\omega + \hat{\omega})/k$. Near resonance ($\hat{\omega} \to \omega$), the amplitude grows as time t and the effective phase speed resembles that of the free wave. However, for the situation where the forcing frequency is considerably less than the frequency of the free waves, such as might occur if the alongshore phase speed of the forcing were small compared to the wave speeds of the low mode free waves, we find $\omega_e \sim \frac{1}{2}\omega$ and $c_e \sim \frac{1}{2}\omega/k = \frac{1}{2}c$. That is, the phase speed of the combined signal diminishes to half that of the free wave alone. This implies that the cross-correlation between two Cartesian velocity series (consisting of an average over all frequency bands) can, in certain instances, yield a phase speed which is half that predicted for a free wave model. Similarly, for the case where the forcing travels much more rapidly than the given free waves, the cross-correlation between two series will produce an effective phase speed that is close to half the alongshore phase speed of the forcing.

c. Traveling wave forcing: Initial start location

Here we consider a traveling wave forcing that is zero beyond some start location $y = 0$:

$$\tau = \begin{cases} \tau_0 \cos(\hat{k}y - \omega t), & y > 0 \\ 0, & y < 0. \end{cases} \tag{4.15}$$

This type of forcing has been considered by Gill and Schumann (1974) and Thomson and Crawford (1982) for wind and tidal current forcing, respectively. The start location in the latter study was actually determined by the position alongshore where diurnal period oscillation could first be supported by the coastal topography. The case $\hat{k} = 0$ for the finite alongshore domain $Y > y > 0$ corresponds to the square wave forcing model considered by Gill and Schumann (where $\omega \to \omega - \pi/2$).

From (2.5) and (4.15) we obtain,

$$\psi(x, y, t) = E_0\phi[F \sin(ky - \omega t - \tilde{\mu}) - \sin(\hat{k}y - \omega t - \tilde{\mu})],$$

where $k = \omega/c$ is the wavenumber of the free wave, $\tilde{\mu} = \tan^{-1}[R/(k - \hat{k})]$ and

$$E_0 = \frac{\tau_0 b}{f\rho_0}\frac{1}{[(\hat{k} - k)^2 + R^2]^{1/2}}.$$

This is distinct from the previous case in that oscillations are at a single frequency and distinct from the square wave forcing because there are two nonzero wavenumbers. Possible resonance at $\hat{k} = k$ is removed by friction. The Cartesian velocity components are

$$U = E_0\phi/H\{F[k \cos(ky - \omega t - \tilde{\mu}) - R \sin(ky - \omega t - \tilde{\mu})] - \hat{k} \cos(\hat{k}y - \omega t - \tilde{\mu}), \tag{4.16a}$$

$$V = -E_0\phi'/H[F \sin(ky - \omega t - \tilde{\mu}) - \sin(\hat{k}y - \omega t - \tilde{\mu})]. \tag{4.16b}$$

The velocity components again consist of damped free and forced waves. For $R = 0$ these reduce to

$$U = e\phi[k \cos(ky - \omega t) - \hat{k} \cos(\hat{k}y - \omega t)], \tag{4.17a}$$

$$V = -2e\phi' \sin\left[\tfrac{1}{2}(k - \hat{k})y\right] \cos\left[\tfrac{1}{2}(\hat{k} + k)y - \omega t\right] \tag{4.17b}$$

in which

$$e = \frac{\tau_0 b}{f\rho_0}\frac{1}{H(k - \hat{k})},$$

and the alongshore component has the form of a spatially modulated traveling wave with effective wavenumber $\frac{1}{2}(\hat{k} + k)$. Near resonance ($\hat{k} \approx k$)

$$(U, V) \approx y[\hat{k}\phi \sin(\hat{k}y - \omega t), \phi' \cos(\hat{k}y - \omega t)]$$

so that the current speeds amplify alongshore from the start location $y = 0$.

The amplitudes and phases of the inviscid rotary constituents are

$$A^{\pm} = e/2\{[(k\phi \pm \phi') - (\hat{k}\phi \pm \phi') \cos(k - \hat{k})y]^2 + (\hat{k}\phi \pm \phi')^2 \sin^2(k - \hat{k})y\}^{1/2}, \quad (4.18)$$

$$\epsilon^{\pm} = \mp\left\{ky + \tan^{-1}\left[\frac{(\hat{k}\phi \pm \phi') \sin(k - \hat{k})y}{(k\phi \pm \phi') - (\hat{k}\phi \pm \phi') \cos(k - \hat{k})y}\right]\right\} + \pi m^{+}. \quad (4.19)$$

The ellipse orientation $\theta = \frac{1}{2}(\epsilon^{+} + \epsilon^{-})$ is then

$$\theta = -\frac{1}{2}\tan^{-1}\left\{\frac{\phi^{2\prime}(k - \hat{k}) \sin(k - \hat{k})y}{(k^2\phi^2 - \phi'^2) + \hat{k}^2\phi^2 - \phi'^2) - 2[k\hat{k}\phi^2 - \phi'^2] \cos(k - \hat{k})y}\right\}. \quad (4.20)$$

For $\hat{k}/k \to 0$, expressions (4.18), (4.19) and (4.20) reduce to their counterparts for square wave forcing, within a difference of $\pi/2$ determined by

$$\tan^{-1}\alpha + \tan^{-1}(1/\alpha) = \frac{\pi}{2}\ (\alpha > 0); = -\frac{\pi}{2}\ (\alpha < 0).$$

The rotary component amplitudes and phases are seen to be nontrivial functions of along and across-shore position. This in turn causes the current ellipse orientation to gradually change in the x, y directions, in contrast to the free wave case where it is either normal or parallel to the coast. As with the free waves, the Cartesian representation is considerably more straightforward than the rotary representation. Moreover, friction is easily included only for the Cartesian components. For example, the alongshore velocity component (4.16b) may be written

$$V = \frac{-E_0\phi'}{H} G \cos\left(\gamma - \omega t + \frac{\pi}{2} - \mu\right),$$

where

$$G = (1 - 2F \cos[(k - \hat{k})y] + F^2)^{1/2},$$

$$\tan\gamma = \frac{\sin\hat{k}y - F \sin ky}{\cos\hat{k}y - F \cos ky}. \quad (4.21)$$

The observed wavenumber k_{cal} of a wave traveling between stations located at y_1 and y_2 is calculated from alongshore velocity components by

$$k_{cal} = \frac{\gamma(y_2) - \gamma(y_1)}{y_2 - y_1} = \frac{\gamma_{21}}{y_2 - y_1}, \quad (4.22)$$

and the wavelength by

$$\lambda_{cal} = \frac{2\pi(y_2 - y_1)}{\gamma_{21}}.$$

Calculated values of wavenumber and wavelength are related to those of free waves through (4.21) and (4.22), taking into account the possible 2π ambiguity in phase when evaluating (4.22). For distances far downstream such that $F \to 0$ then $\gamma = \hat{k}y$ and $k_{cal} = \hat{k}$ (the forcing wavenumber). The response therefore travels with the forcing and is phase locked with phase difference $\pi/2 - \mu$.

We noted previously that the square-wave forcing model is obtained in the limit $\hat{k}/k \to 0$. The velocity components (4.17a, b) are then,

$$\left.\begin{aligned} U &= \tilde{e}\phi k \cos(ky - \omega t) \\ V &= -2\tilde{e}\phi' \sin\left(\frac{1}{2}ky\right) \cos\left(\frac{1}{2}ky - \omega t\right) \end{aligned}\right\},$$

for which $\tilde{e} = \tau_0 b/(f\rho_0 kH)$. The phases (3.4) for the alongshore and cross-shore components are therefore

$$\gamma_{21}^{\pm} = \mp\frac{1}{2}k(y_2 - y_1), \quad \gamma_{21}^{\pm} = \pm k(y_2 - y_1)$$

respectively. Thus if the V component is used to determine the alongshore wavenumber we find that the calculated wavelength

$$\lambda_{cal} = \frac{2\pi}{|\gamma_{21}^{\pm}|}(y_2 - y_1)$$

is related to the wavelength λ of the free wave component by

$$\lambda = \frac{2\pi}{|\gamma_{21}^{\pm}|}(y_2 - y_1) = \frac{1}{2}\lambda_{cal}.$$

That is, the wavelength calculated using the phase difference and alongshore distance is twice that of the free wave solution. If the U component is used, $\lambda = \lambda_{cal}$.

5. Application of results

To this point, we have dealt mainly with the generalized properties of shelf waves. We now apply the results to a specific case. In particular we are concerned with the spatial variability of rotary phases, $\epsilon^{\pm}$, and the ellipse orientation, $\theta = \frac{1}{2}(\epsilon^{+} + \epsilon^{-})$, for first-mode, prograde waves of diurnal (K_1) frequency propagating along a continental margin of uniform topography. Observed waves of this type have been described by Thomson and Crawford (1982) and by

Crawford and Thomson (1982, 1984) for the continental margin of Vancouver Island, British Columbia.

The wavenumber k for first mode shelf waves of K_1 frequency (ω = 0.0417 cph) has been obtained from the calculated dispersion curve $\omega(k)$ for the specified shelf-slope topography appropriate to the central coast of Vancouver Island, (Fig. 2a). We then used this value of k (e.g., Henry *et al.*, 1985) to derive the cross-shelf values of ϕ and ϕ' at one kilometer intervals seaward of the coast. The cross-shore variation in the ratio $k\phi/\phi'$ needed in the analysis is presented in Fig. 2b.

The rotary phases and ellipse orientation for freely propagating, frictionally damped waves are given by (4.4) and (4.6), respectively. Frictional effects arise solely through the inverse tangent functions whose amplitudes versus cross-shore location x/L are plotted in Figs. 3 and 4 for three values of R/k. At the coast, $\phi = 0$, so rotary phases and ellipse orientations are identical to those of the inviscid case. Seaward of the coast, however, the effects of viscous induced phase shifts become increasingly important.

In the nearshore and deep-sea regions (where $|k\phi/\phi'| < 1$), the current ellipses for free inviscid waves are parallel to the coast ($m = 1$) while in the slope region (where $|k\phi/\phi'| > 1$) they are normal to the coast ($m = 0$). For $R/k \ll 1$, the offshore locations where these ellipses change orientation is almost coincident with the zeroes of $(k^2 + R^2)\phi^2 - (\phi')^2$ in (4.6). Consequently, friction only slightly alters the locations of major ($\approx$90°) ellipse reorientation. Taking $m^+ \equiv 0$ and $m^- = m$ in (4.4), we see that ϵ^+ has a 180° discontinuity at $k\phi = -\phi'(x/L \approx -0.43)$ while ϵ^- is discontinuous at $k\phi = \pm\phi'$, as in the inviscid case (Hsieh, 1982a). In summary, frictional terms have a major effect on the basic patterns of rotary phases and ellipse orientation and lead to significant ($\approx$10°) cross-shore phase lags and cross-isobath ellipse alignments.

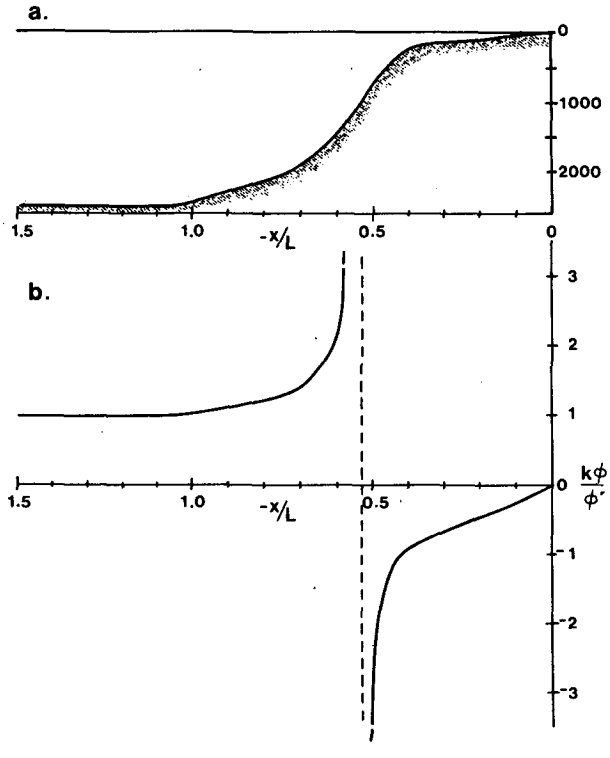

FIG. 2. Cross-shore depth profile (a) and corresponding velocity component ratio $k\phi/\phi' \sim u/V$ (b) for first mode diurnal period continental shelf waves of frequency ω = 0.0417 cph (1.16×10^{-5} s^{-1}) and free wavenumber $k = 3.9 \times 10^{-5}$ m^{-1}. The shelf width $L = 10^5$ m.

We now consider the case of inviscid, tidally-forced shelf waves of diurnal frequency. Because the wavelength of the tidal forcing (10^4 km) is so much greater than that of the free waves (10^2 km), the limit $\hat{k}/k \to 0$ applies in (4.19) and (4.20), whereby

$$\epsilon^{\pm} = \mp ky - \tan^{-1}\left[\frac{\sin ky}{(k\phi/\phi' \pm (1 - \cos ky)}\right], \quad (5.1)$$

$$\theta = -\frac{1}{2}\tan^{-1}\left[\frac{(2k\phi/\phi')\sin ky}{(k\phi/\phi')^2 - 2(1 - \cos ky)}\right] + \frac{1}{2}m\pi. \quad (5.2)$$

The corresponding expressions for the free waves are given by (4.4) and (4.6) with $R = 0$ or by (5.1) and (5.2) with $\tan^{-1}[\cdot] = 0$.

For free inviscid waves, the principal parts of the anticlockwise and clockwise rotary phase angles are $\epsilon^{\pm} = \mp ky$ and co-phase lines are perpendicular to the coast (dotted lines in Figs. 5 and 6). It is this form for the waves that is used in the analysis by Crawford and Thomson (1982, 1984). Addition of the forced wave component modifies the phase lines such that at only one offshore location—where the alongshore velocity component vanishes (i.e., $\phi' = 0$) and $k\phi/\phi'$ changes sign—are the phases of the forced and free waves equal for all ky. In the present example, this occurs near 53 km offshore ($x/L = -0.53$). Moreover, there are discontinuities in the phase angles brought about by zeroes of the denominator $\delta^{\pm} = k\phi/\phi' \pm (1 - \cos ky)$ in (5.1). For a fixed value of $k\phi/\phi'$ (i.e., fixed offshore distance), singularities in $\epsilon^{\pm}$ occur in pairs symmetric about $ky = \pi$.

In the case of ϵ^+ (Fig. 5), discontinuities in phase are found over the continental shelf region in the zone $-2 < k\phi/\phi' < 0$, approximately between the coast and 45 km offshore (cf., Fig. 2b). Except for the vicinity of the discontinuities the anticlockwise rotary phase changes little with location. Seaward of this, however, ϵ^+ varies continuously. In contrast, the clockwise rotary phase (Fig. 6) is continuous in the regions $k\phi/\phi' < 0$ and $k\phi/\phi' > 2$ which spans the continental shelf and part of the slope out to about 62 km. Seaward of this location, ϵ^- is discontinuous with phase values actually decreasing with increasing

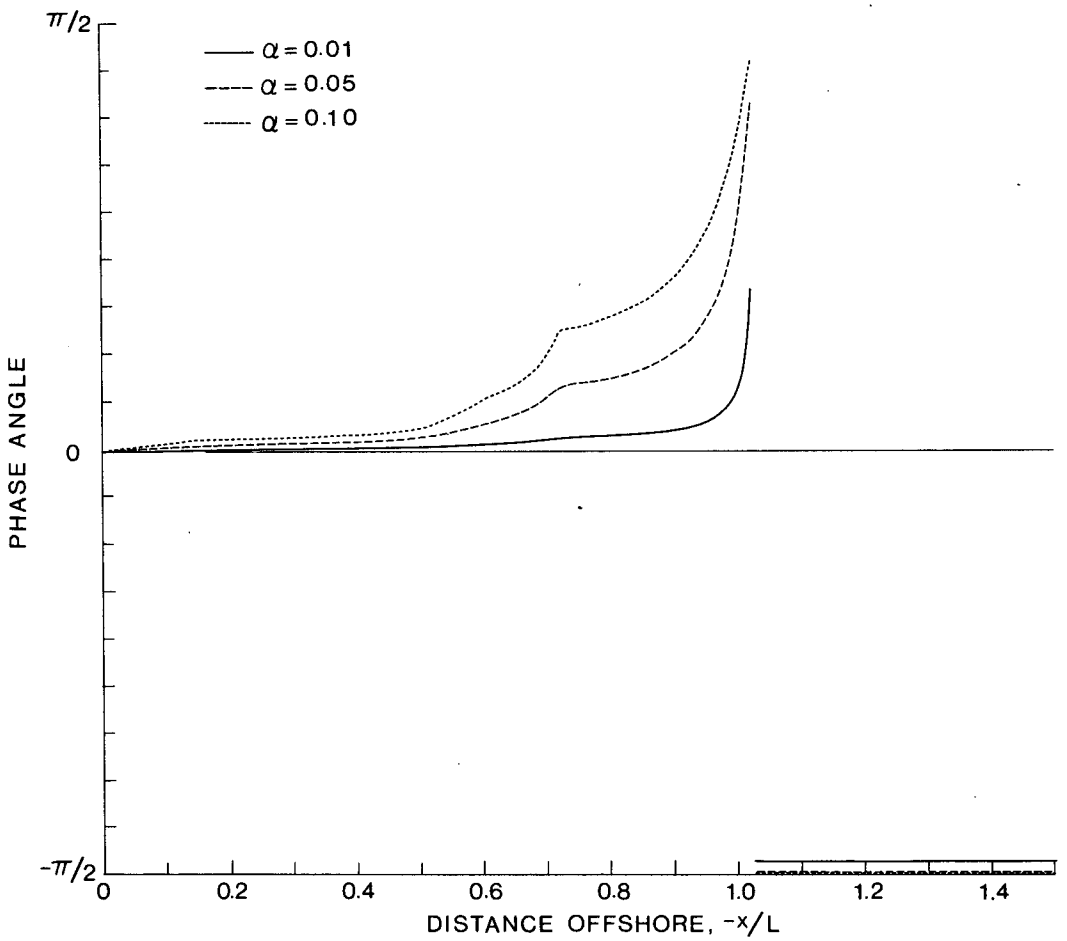

FIG. 3. Friction induced phase modifications versus cross-shore location due to the inverse tangent function in (4.8) for the clockwise rotary phase, ϵ^- for first mode diurnal period shelf waves (cf. Fig. 2). $\alpha = R/k$ where k is the wavenumber of the free wave component and R is the friction coefficient.

ky for alongshore location in the range $\pi/2 < ky < 3\pi/2$.

These results makes it clear that it is best to use the phase angle which is continuous in the region of interest when attempting to use the rotary properties of currents to estimate the wavenumbers k from a set of observations. Here, for instance, estimates would be based on ϵ^- for measurements from the shelf and inner slope regions and off Vancouver Island on ϵ^+ if they were from the outer slope-region. The most reliable estimates would be for currents measured on the inner shelf where the V-component of the shelf-wave current is large ($k\phi/\phi' \ll 1$) rather than seaward of the shelf break where it is small. However, even over the inner shelf, the basic nonlinearity of the rotary angles as a function of position means that conversion of the phase differences (3.4) into values for k or wavelength λ cannot, in general, be based on (4.10) or (4.11). In the present case, for example, ϵ^- changes rapidly ($\approx 90°$) near the ends of the interval $0 \leq ky \leq 2\pi$ for the zone adjacent to the coast. Away from the ends of the interval, we find $\gamma_{21}^- \approx \alpha k(y_2 - y_1)$ for a fixed distance offshore in this zone with $\frac{1}{2} \leq \alpha(x) \leq 1$ (Fig. 7). Thus, if we had measured γ_{21}^- directly for this particular frequency band and then converted it to a calculated wavelength using the free wave relation (4.11) we would obtain $\lambda_{cal} = \alpha^{-1}\lambda$ where λ is the free wave length. In the nearshore limit $\alpha \approx \frac{1}{2}$, and the "measured" wavelength for the free wave component of the forced wave would be estimated as $2\lambda = 2(2\pi/k) \approx 320$ km rather than the actual value of 160 km. Only for observations taken near the offshore region where $\phi' = 0$ would we have derived the correct value for λ. Using values of ϵ^- derived from moored current meter records, Crawford and Thomson (1982, 1984) find that the "observed" wavelengths of first mode K_1 waves off central Vancouver Island range from 200 km in summer to 235 km in winter. The authors link the discrepancy between these observed values and the wavelength of 160 ± 10 km obtained from the unforced, barotropic wave model to baroclinic

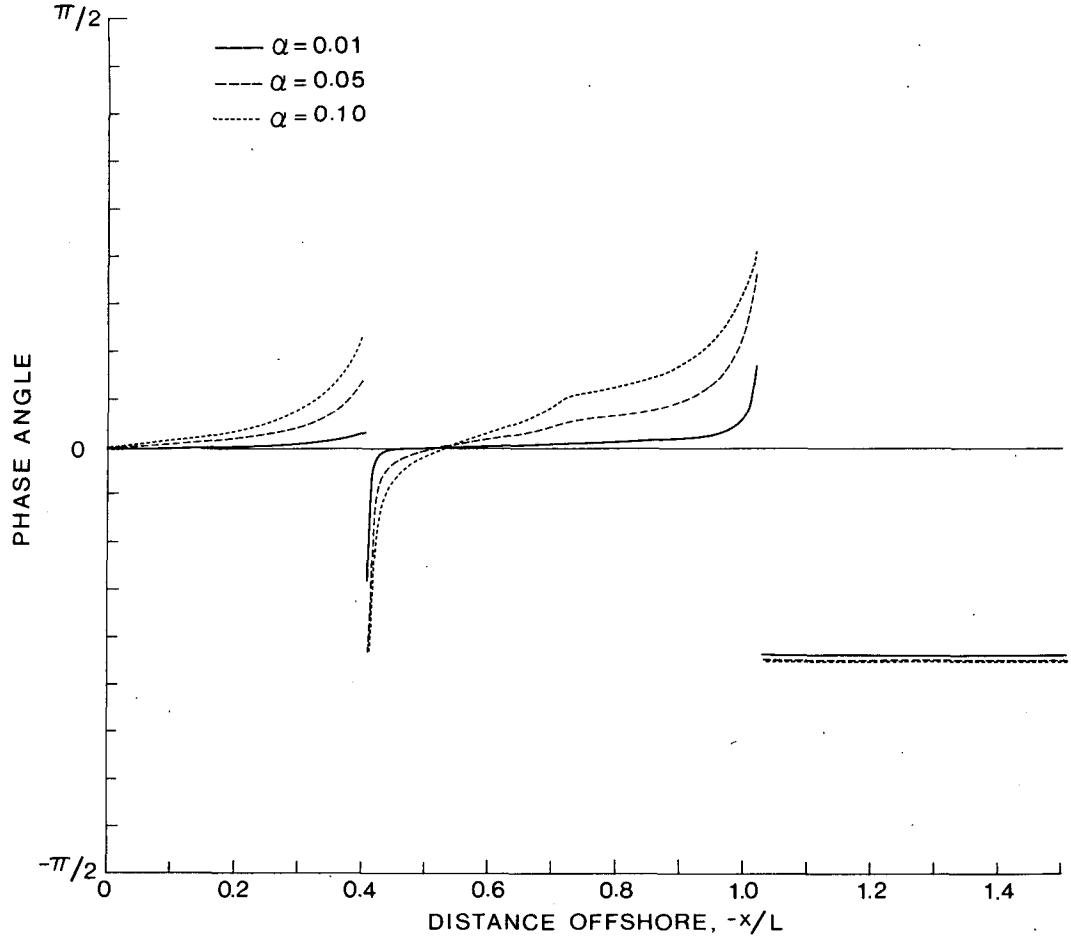

FIG. 4. Friction induced modifications to the ellipse orientations versus cross-shore location due to the inverse tangent function in (4.6). Compare with Fig. 3.

effects and to seasonal variations due to changes in the prevailing alongshore current. Our analysis suggests an alternate explanation for at least part of the discrepancy; namely, that there is also a forced wave component off Vancouver Island. In this case, the assumption that lines of constant phase ϵ^- are perpendicular to the coast is no longer valid. If we assume that the shelf waves have a start location off Juan de Fuca Strait, then the summer and winter wavelengths correspond to ϵ^- values of 320° and 274°, respectively. These angles, combined with Figs. 6 and 7 and the fact that the observed values are based on current meter measurements at the offshore location $-x/L \sim 0.13$, yield respective alongshore distances, ky, of 350° and 320° (see dotted lines in Fig. 7). From the latter angles, we estimate that the free wave componennt of K_1 shelf waves off Estevan Point has a wavelength of 180 km in summer and 200 km in winter. These estimates from the forced wave model are about 10–15% less than the wavelengths based on the free wave model and much more closely approximate the predicted 160 km wavelength of the free-wave component for the central portion of Vancouver Island. Thus, baroclinic and advective effects are presumably still important but not to the extent required by the free wave model.

Current ellipse orientations are given (5.2) or by its equivalent expression $\theta = \frac{1}{2}(\epsilon^+ + \epsilon^-)$. Free shelf wave ellipses are parallel to the coast ($m = 1$) within 40 km of shore and seaward of 100 km, and normal to the coast ($m = 0$) between 40 and 100 km offshore. The pattern is considerably more complex for the forced wave response and ellipse orientations depart by as much as 45° from along or across-shore orientations. Only near $ky = p\pi$ ($p = 0, 1, \cdots$), at the coast $x/L = 0$ (where $\phi = 0$) and at the offshore distance where $\phi' = 0$ are forced wave ellipses aligned in the same direction as the free wave ellipses.

The previous results point to an obvious difficulty in any real application of rotary components to forced wave models: determination of the reference location $y = 0$. If, as is usually the case, this is not known with any accuracy then measured angles (ϵ^+, ϵ^-, θ) must be fitted to maps like those constructed

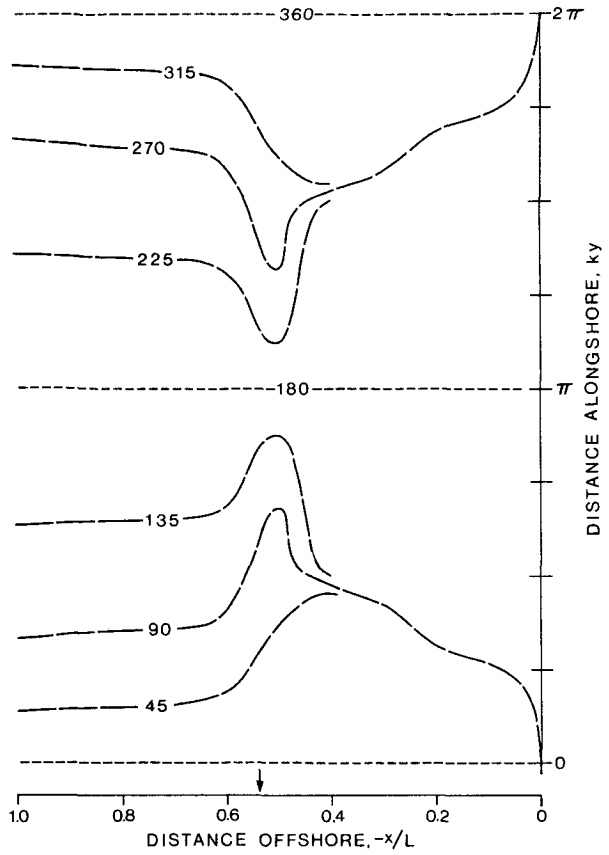

FIG. 5. The principal part of the rotary phase ϵ^+ (i.e., $m^+ \equiv 0$) for the interval $0 \leq ky \leq 2\pi$ and $-1.0 \leq x/L \leq 0$ for forced first mode diurnal period shelf waves (5.1). Arrow indicates where $\epsilon^+ = -ky$. Values in degrees.

in Figs. 5 and 6 in order to determine the locations of current meter moorings in the intervals $2\pi m \leq ky \leq 2\pi(m + 1)$. The start location $y = 0$ is therefore implied from the observations. For free waves no such difficulty arises; co-phase lines are equally spaced throughout the interval and (4.10, 4.11) can be applied directly. Finally, we note that the spatial patterns of ϵ^+, ϵ^- and θ associated with forced waves could be confused with those of free waves modified by friction if data are available for only a few locations alongshore. As for the case off Vancouver Island, further complications arise because of changes in topography, coastline curvature and stratification.

6. Discussion and summary

Forced barotropic continental-shelf waves have an alongshore structure that is strongly dependent upon the salient features of the forcing. A determination of the alongshore wavenumber dependence, in conjunction with the across-shelf structure, provides a full description of the forced barotropic shelf-wave response. In this paper, we have outlined methods by which wavenumbers (and hence wavelengths and wave speeds) calculated from data by Fourier analysis techniques may be related to the wavenumbers of the free wave components of selected types of forced shelf waves. Frictional modifications of the response is addressed assuming frictional forces are small and linearly dependent on alongshore velocity. The resulting wavenumber dependence is compared with that of the undamped case. While not all of the work presented here is new in terms of forced shelf wave theory, we provide a detailed investigation of the alongshore wave structure that is relevant to a practical comparison of theory with measurement. Our results clearly emphasize the importance of knowing the wavenumber–frequency distribution of the alongshore forcing mechanism.

Both rotary and Cartesian current representations are considered. Provided the alongshore direction is readily specified (which requires relatively straight topographic contours and coastline), there are substantial advantages to using Cartesian components because of the simplified algebra. This is particularly

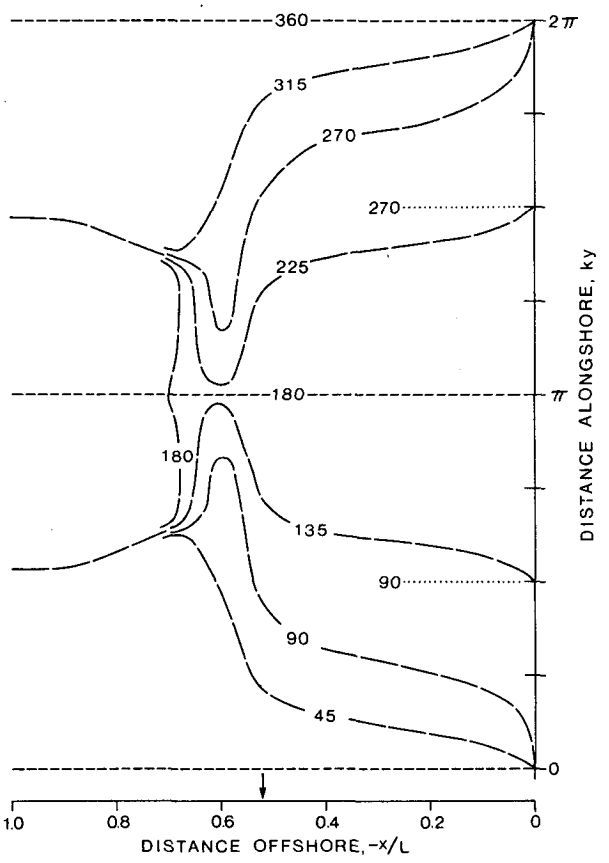

FIG. 6. The principal part of the rotary phase ϵ^- (i.e., $m^- \equiv 0$) for the interval $0 \leq ky \leq 2\pi$ and $-1.0 \leq x/L \leq 0$ for forced first mode diurnal period shelf waves (5.1). Arrow indicates where $\epsilon^- = ky$. Values in degrees.

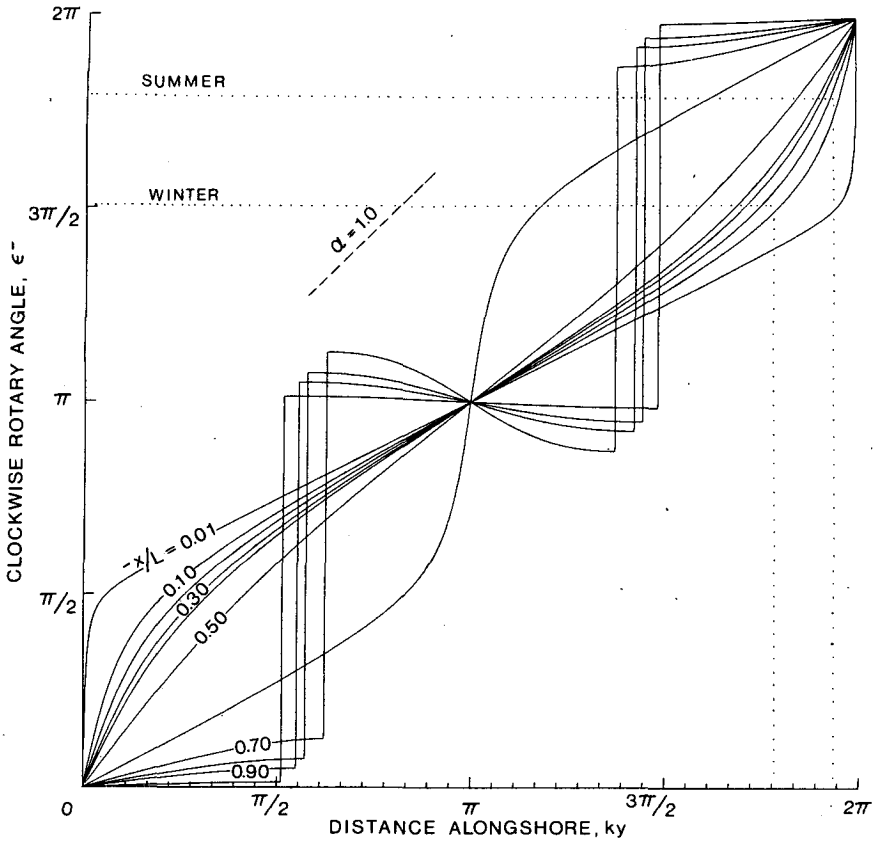

FIG. 7. The principal part of the rotary phase ϵ^- versus alongshore position ky for various offshore locations x/L for the waves in Fig. 6. $\alpha = \Delta\epsilon^-/\Delta ky$ is the slope of the curve, with $\alpha = 1$ shown by the dashed line. $L = 10^5$ m. Dotted lines are for wavelength estimates described in Section 5.

true for the alongshore components because their amplitudes are much greater than across-shore components over much of the continental shelf. The higher signal to noise ratio for the alongshore flow over the inner shelf leads to improved reliability in phase and, subsequently, wavenumber estimates.

The techniques of rotary cross-spectral analysis between vector series permit calculation of current ellipse orientation and differences in rotary component phases between currents at different locations. For cases where the coastline changes significantly over a wavelength or for offshore regions where there is possible ambiguity in defining the "alongshore" direction, rotary coherence analysis provides a more reliable method for calculating phase differences than Cartesian coherence analysis. However, considerable care is required if observations are to be correctly interpreted. In particular, there is a preferred direction of current vector rotation leading to more nearly circular ellipses seaward over the shelf. Consideration of phase differences between rotary components having the preferred direction of rotation will yield more reliable estimates of phase lag owing to the continuous spatial structure of phases in the region. The phase of the oppositely rotating component, on the other hand, has 180° discontinuities combined with small spatial gradients in this region. The results presented for the specific example of tidal-forced, first-mode shelf waves of diurnal period details some of the pitfalls associated with the rotary analysis for forced waves.

Finally, it is appropriate to note the important effect that friction has on the amplitudes and phases of the response in all examples given here. In particular the effect of friction removes resonant singularities from the solution and damps the free wave contributions. However, the presence of the free and forced frequencies (ω and $\hat{\omega}$) in the amplitude denominator of the impulse start time problem, and the presence of the free and forced wavenumbers (k and $\hat{k}$) in the amplitude denominator of the initial start location problem are also important. Estimates of the friction coefficient obtained from an assumed shallow-water wind stress/bottom friction balance (Winant and Beardsley, 1979) range widely and this may well be due to these additional terms in the denominator, which are not always small compared with the friction term in wind-forced waves.

Acknowledgments. This work was partially supported by the Australian Marine Sciences and Technologies Grants Scheme under Grant MST 81/0342.

REFERENCES

Adams, J. K., and V. T. Buchwald, 1969: The generation of continental shelf waves. *J. Fluid Mech.*, **35,** 815–826.

Allen, J. S., 1980: Models of wind-driven currents on the continental shelf. *Annual Review of Fluid Mechanics,* Vol. 12, Annual Reviews, 389–433.

Brink, K. H., 1982: The effect of bottom friction on low-frequency coastal trapped waves. *J. Phys. Oceanogr.*, **12,** 127–133.

——, and J. S. Allen, 1978: On the effect of bottom friction on barotropic motion over the continental shelf. *J. Phys. Oceanogr.*, **8,** 919–922.

——, and ——, 1983: Reply to T. J. Simons. *J. Phys. Oceanogr.*, **13,** 149–150.

Calman, J., 1978: On the interpretation of ocean current spectra. *J. Phys. Oceanogr.*, **8,** 627–652.

Crawford, W. R., and R. E. Thomson, 1982: Continental shelf waves of diurnal period along Vancouver Island. *J. Geophys. Res.*, **87,** 9516–9522.

——, and ——, 1984: Diurnal period continental shelf waves along Vancouver Island: A comparison of observations with numerical models. *J. Physical Oceanogr.*, **14,** 1629–1646.

Csanady, G. T., 1978: The arrested topographic wave. *J. Phys. Oceanogr.*, **8,** 47–62.

Gill, A. E., and E. H. Schumann, 1974: The generation of long shelf waves by the wind. *J. Phys. Oceanogr.*, **4,** 83–90.

Hamon, B. V., 1962: The spectrums of mean sea level at Sydney, Coffs Harbour and Lord Howe Island. *J. Geophys. Res.*, **67,** 5147–5155.

Henry, R. F., W. R. Crawford and R. E. Thomson (in preparation). Calculation of dispersion curves and modal shapes of continental shelf waves.

Hsieh, W. W., 1982a: On the detection of continental shelf waves. *J. Phys. Oceanogr.*, **12,** 414–427.

——, 1982b: Observations of continental shelf waves off Oregon and Washington. *J. Phys. Oceanogr.*, **12,** 887–896.

Koopmans, L. H., 1974: *The Spectral Analysis of Time Series.* Academic Press, 366 pp.

Middleton, J. H., 1982: Outer rotary cross spectra, coherences and phases. *Deep-Sea Res.* **29,** 1267–1269.

——, 1983: Low frequency trapped waves on a wide reef-fringed continental shelf. *J. Phys. Oceanogr.*, **13,** 1371–1382.

——, T. D. Foster and A. Foldvik, 1982: Low frequency currents and continental shelf waves in the Southern Weddell Sea. *J. Phys. Oceanogr.*, **12,** 618–634.

Mooers, C. N. K., 1973: A technique for the cross spectrum analysis of pairs of complex-valued time series, with emphasis on properties of polarized components and rotational invariants. *Deep-Sea Res.*, **20,** 1129–1141.

Mysak, L. A., 1980: Recent advances in shelf wave dynamics. *Rev. Geophys. Space Phys.*, **18,** 211–241.

Simons, T. J., 1983: Comments "On the effect of bottom friction on continental shelf waves," *J. Phys. Oceanogr.*, **13,** 147–148.

Thomson, R. E., and W. R. Crawford, 1982: The generation of diurnal period shelf waves by tidal currents. *J. Phys. Oceanogr.*, **12,** 635–643.

Winant, C. D., and R. C. Beardsley, 1979: A comparison of some shallow wind driven currents. *J. Phys. Oceanogr.*, **9,** 218–220.